Front. Chem. Sci. Eng. 2022, 16(12): 1700−1712
https://doi.org/10.1007/s11705-022-2207-6

RESEARCH ARTICLE

Thermodynamic analysis of reaction pathways and equilibrium yields for catalytic pyrolysis of naphtha

Dongyang Liu, Yibo Zhi, Yuen Bai, Liang Zhao (✉), Jinsen Gao, Chunming Xu

State Key Laboratory of Heavy Oil Processing, China University of Petroleum (Beijing), Beijing 102249, China

Abstract The chain length and hydrocarbon type significantly affect the production of light olefins during the catalytic pyrolysis of naphtha. Herein, for a better catalyst design and operation parameters optimization, the reaction pathways and equilibrium yields for the catalytic pyrolysis of C_{5-8} *n*/*iso*/cyclo-paraffins were analyzed thermodynamically. The results revealed that the thermodynamically favorable reaction pathways for *n*/*iso*-paraffins and cyclo-paraffins were the protolytic and hydrogen transfer cracking pathways, respectively. However, the formation of light paraffin severely limits the maximum selectivity toward light olefins. The dehydrogenation cracking pathway of *n*/*iso*-paraffins and the protolytic cracking pathway of cyclo-paraffins demonstrated significantly improved selectivity for light olefins. The results are thus useful as a direction for future catalyst improvements, facilitating superior reaction pathways to enhance light olefins. In addition, the equilibrium yield of light olefins increased with increasing the chain length, and the introduction of cyclo-paraffin inhibits the formation of light olefins. High temperatures and low pressures favor the formation of ethylene, and moderate temperatures and low pressures favor the formation of propylene. *n*-Hexane and cyclohexane mixtures gave maximum ethylene and propylene yield of approximately 49.90% and 55.77%, respectively. This work provides theoretical guidance for the development of superior catalysts and the selection of proper operation parameters for the catalytic pyrolysis of C_{5-8} *n*/*iso*/cyclo-paraffins from a thermodynamic point of view.

Keywords naphtha, catalytic pyrolysis, reaction pathway, equilibrium yield

Received April 25, 2022; accepted June 2, 2022

E-mail: liangzhao@cup.edu.cn

1 Introduction

Light olefins, such as ethylene, and propylene, are important chemical intermediates in the field of organic synthesis, and global demand for them is large and demonstrates an increasing trend [1–3]. In the past decades, light olefins have usually been obtained via the steam cracking of naphtha, which suffers from high reaction temperatures (over 800 °C), high energy consumption, and difficulty in adjusting the propylene/ethylene ratio [4,5]. In contrast, the catalytic pyrolysis of naphtha is expected to improve the yield of light olefins in the future owing to its lower reaction temperature and adjustable product selectivity [6,7]. Effective shape-selective catalysts are important for the catalytic pyrolysis of naphtha, as they can accelerate the cracking reaction of feedstocks and improve the yields of light olefins [8,9]. ZSM-5 and metal-containing ZSM-5 zeolite catalysts are representative catalysts for the catalytic pyrolysis of naphtha, and they have been widely studied [10,11].

It is well known that the catalytic pyrolysis of hydrocarbons follows the carbenium ion mechanism over HZSM-5 zeolites [12–15]. Hydrocarbon activation is an important step in the catalytic pyrolysis of the naphtha to produce light olefins, this step is primarily catalyzed by Brønsted acid sites over HZSM-5 zeolites [16,17]. The activation modes of hydrocarbons are divided into protolytic cracking (the proton attacks the C–C bond), dehydrogenation (the proton attacks the C–H bond), and hydride/hydrogen transfer activations (the conversion between paraffins and olefins). Therefore, the cracking process is divided into three reaction pathways: the protolytic cracking pathway, the dehydrogenation cracking pathway, and the hydride/hydrogen transfer cracking pathway [18–20]. Hou et al. [21] analyzed the reaction pathways of *n*-pentane over HZSM-5 zeolites to produce light olefins, they concluded that the reaction pathway of *n*-pentane significantly affects the formation of light olefins. Therefore, it is necessary to clarify and

promote the optimal reaction pathway for the catalytic pyrolysis of naphtha to enhance the yield of light olefins.

Apart from the reaction pathway, the operation parameters also significantly affect the yields of light olefins [22–24]. Wattanapaphawong et al. [2] investigated the effect of the C_{5-8} *n*-paraffins on the yield of light olefin by catalytic pyrolysis at 923 K and 873 K, they suggested that the cracking performance at high temperatures is significantly different from that at low temperatures. The pressure effects on pyrolysis of *n*-decane were investigated by Wang et al. [25], they concluded that pressure weakens the formation of light olefins. Most studies in the literature have focused on *n*-paraffins because naphtha is a mixture of hydrocarbons, and its primary components are *n*-paraffins [26–28]. Although cyclo-paraffins are important constituents of naphtha, and their cracking product distribution is quite different from that of *n*-paraffin cracking, fewer studies on the cracking of cyclo-paraffin have been published.

However, the investigation of the optimal reaction pathways and operation parameters for hydrocarbons with different chain lengths and types remains a challenge via the experimental method, owing to the complexity of the naphtha composition [29–31]. The thermodynamic method is a better approach to studying the superior pathway of *n*/*iso*/cyclo-paraffin catalytic pyrolysis to enhance the yield of light olefins based on reaction enthalpy and equilibrium constant. As for operating parameters, Zhu et al. [32] investigated the effects of operation parameters on the thermodynamic equilibrium yield, and the results showed that the yields of light olefins were restricted by operation parameters. Therefore, it is feasible to establish a reasonable thermodynamic model to optimize the operation parameters for enhancing light olefins. Stoichiometric and non-stoichiometric approaches are typically applied to thermodynamic equilibrium analysis [33,34]. Because of the complexity of the reaction system, the non-stoichiometric approach, namely the Gibbs free energy minimization method, is more suitable. Moreover, the effects of the chain length of reactant and cyclo-paraffin content on the production of light olefins have not yet been studied in detail using the thermodynamic method.

Understanding the superior reaction pathway and thermodynamic equilibrium yield of C_{5-8} *n*/*iso*/cyclo-paraffins is important for developing the catalytic pyrolysis process of naphtha. In this study, C_{5-8} *n*/*iso*/cyclo-paraffins were selected as model reactants for an analysis of the catalytic pyrolysis process and the effects of different reaction pathways on the formation of light olefins. The Gibbs free energy minimization method was used to study the thermodynamic equilibrium yield at different reaction temperatures and total hydrocarbon pressures using the Aspen Plus software. The effects of the hydrocarbon type, chain length, and hydrocarbon content are also considered in the model. Thus, overall, this study aims to provide theoretical guidance for enhancing the yield of light olefins.

2 Methodology

2.1 Feedstocks and transformation pathways

C_{5-8} *n*/*iso*/cyclo-paraffins are important and representative naphtha compositions. For the sake of brevity, isomers with similar structures were grouped into single species and selected as the object of thermodynamic calculations, because the physical properties of the respective isomers of hydrocarbons are relatively similar [35]. The simplified feedstocks are listed in Table 1.

In this study, the protolytic, dehydrogenation, and hydride transfer cracking pathways of *n*/*iso*-paraffins were considered as shown in Scheme 1 [20]. (1) Protolytic cracking pathway: the H^+ proton attacks the C–C bond to generate tricoordinated carbenium ions and light paraffins. (2) Dehydrogenation cracking pathway: the proton attacks the C–H bond, producing tricoordinated carbenium ions and H_2. (3) Hydride transfer cracking pathway: reactants and $R_1^+Z^-$ carbenium ions over HZSM-5 undergo a hydride transfer reaction to form tricoordinated carbenium ions and R_1H paraffin. Subsequently, the tricoordinated carbenium ions form olefins and new carbenium ions via β-scission. The desorption of tricoordinated carbenium ions in the above three pathways from the active site of catalysts accompanies the regeneration of H^+ proton sites and the formation of light olefins.

Scheme 2 illustrates the reaction pathways for the cyclo-paraffins considered in this study. As can be observed, H^+ attacks cyclo-paraffins, resulting in the formation of pentacoordinated carbonium ion, which

Table 1 Feedstocks composition after simplification

C_{5-8} *n*-paraffin Species		C_{5-8} *iso*-paraffin Species		C_{5-8} cyclo-paraffin	
Formula	Species	Formula	Species	Formula	Species
C_5H_{12}	*n*-Pentane	C_5H_{12}	2-Methylbutane	C_5H_{10}	Cyclopentane
C_6H_{14}	*n*-Hexane	C_6H_{14}	2-Methylpentane	C_6H_{12}	Cyclohexane
C_7H_{16}	*n*-Heptane	C_7H_{16}	2-Methylhexane	C_7H_{14}	Methylcyclohexane
C_8H_{18}	*n*-Octane	C_8H_{18}	2-Methylheptane	C_8H_{16}	Ethylcyclohexane

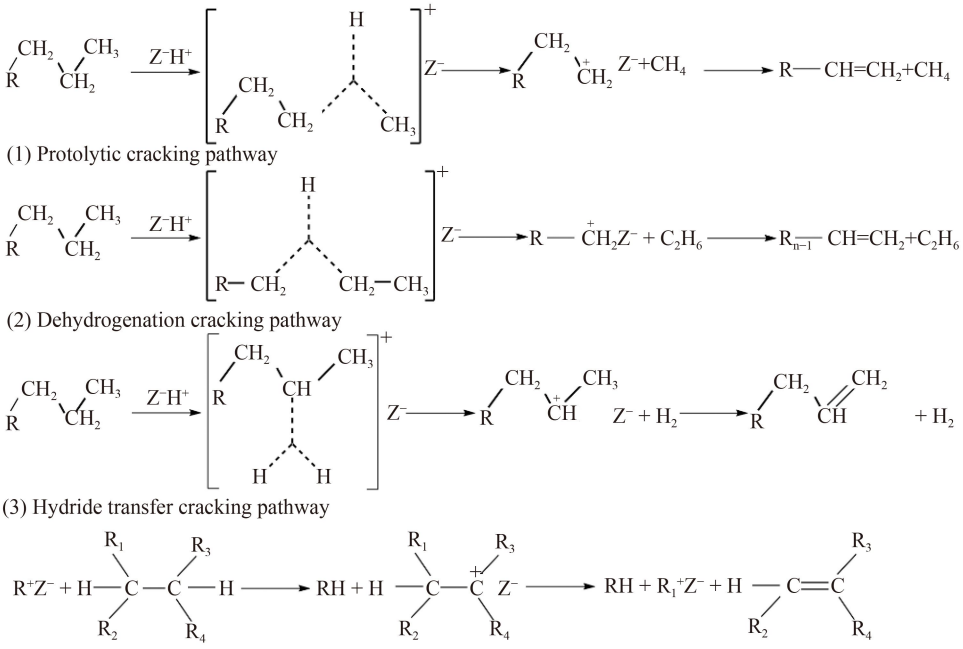

Scheme 1 Reaction pathways of *n*-paraffins and *iso*-paraffins.

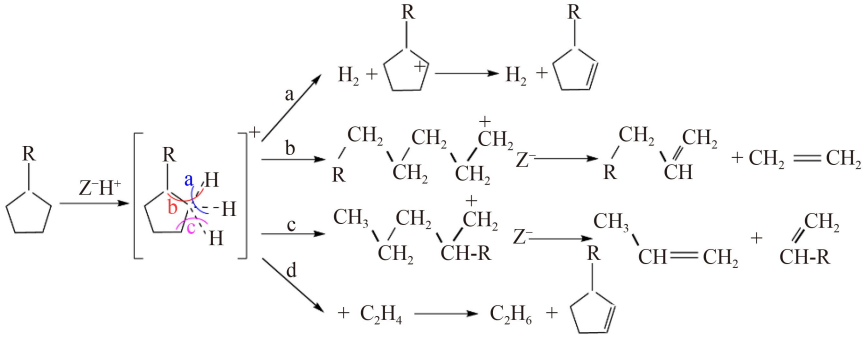

(a) Dehydrogenation cracking pathway; (b,c) Protolyric cracking pathway; (d) Hydrogen transfer cracking pathway

Scheme 2 Reaction pathways of cyclo-paraffins.

undergoes three reaction pathways: (1) dehydrogenation cracking pathway: the cleaved of C–H bonds in pentacoordinated carbocations to form hydrogen and cycloolefins; (2) protolytic cracking pathway: C–C bonds in pentacoordinated carbonium ion is cleaved to form two olefin molecules; (3) hydrogen transfer cracking pathway: hydrogen transfer between carbocations and olefins, leading to the formation of small paraffins and cycloolefins.

Accordingly, the chemical reactions of different reaction pathways for *n*/*iso*/cyclo-paraffin with different carbon numbers and types were established. The stoichiometric coefficients of the reactant molecules in the relevant equations are all one. It is worth noting that light olefins are all derived from the deprotonation and *β*-cracking of stable carbenium ions, the paraffins and olefins in the product are considered *n*-paraffins, 2-methyl-paraffins, and alpha-olefins. The detailed reaction classes and chemical reactions included in this study are provided in Table S1 (cf. Electronic Supplementary Material, ESM).

2.2 Calculation of thermodynamic properties

Based on the chemical reactions of reaction pathways for *n*/*iso*/cyclo-paraffin with different carbon numbers and types. The standard molar formation enthalpy and the standard molar formation entropy for reaction temperature T can be calculated using the following equations:

$$\Delta_f H_m^\theta = \Delta_f H_m^\theta(298.15\ \mathrm{K}) + \int_{298.15}^{T} C_{p,m}\mathrm{d}T, \quad (1)$$

$$\Delta_f S_m^\theta = \Delta_f S_m^\theta(298.15\ \mathrm{K}) + \int_{298.15}^{T} \frac{C_{p,m}}{T}\mathrm{d}T. \quad (2)$$

The contribution value ($C_{p,m,i}$) of each group to the heat capacity at constant pressure for the standard state ($C_{p,m}$) at different temperatures can be obtained using the

Benson group contribution method [36,37], and the $C_{p,m}$ of each species at different temperatures can be calculated using Eq. (3):

$$C_{p,m} = \sum_i N_i C_{p,m,i}. \quad (3)$$

The $C_{p,m}$ for the standard state was formulated as a polynomial equation of order four (five constants) using the regression of $C_{p,m}$ against temperature.

$$C_{p,m} = a_1 + a_2 T + a_3 T^2 + a_4 T^3 + a_5 T^4. \quad (4)$$

According to Eqs. (1)–(4), the standard molar reaction enthalpy, standard molar reaction entropy, and standard molar reaction Gibbs free energy at reaction temperatures T can be obtained and represented as Eqs. (5)–(7).

$$\Delta_r H_m^\theta(T) = \sum_{Product} \Delta_f H_m^\theta(T) - \sum_{Reactant} \Delta_f H_m^\theta(T), \quad (5)$$

$$\Delta_r S_m^\theta(T) = \sum_{Product} \Delta_f S_m^\theta(T) - \sum_{Reactant} \Delta_f S_m^\theta(T), \quad (6)$$

$$\Delta_r G_m^\theta(T) = \Delta_r H_m^\theta(T) - T\Delta_r S_m^\theta(T). \quad (7)$$

In addition, the standard equilibrium constant can be expressed as Eq. (8).

$$K^\theta(T) = \exp\frac{-\Delta_r G_m^\theta}{RT}. \quad (8)$$

2.3 Thermodynamic equilibrium analysis

The non-stoichiometric Gibbs free energy minimization method was used to calculate the thermodynamic equilibrium yield of the catalytic pyrolysis of naphtha. The total Gibbs free energy of the system can be defined as follows [38,39]:

$$G_t = \sum_{i=1}^{M} n_i \mu_i. \quad (9)$$

In the thermochemical equilibrium state, the total Gibbs free energy of the system is minimum; thus, the calculation of the thermodynamic equilibrium yield is an optimization problem, wherein the constraint is the element equilibrium [40]. The most commonly used optimization algorithm is the Lagrange multiplier approach, which can be performed as follows [41]:

$$F = G_t + \sum_{k=1}^{l} \lambda_k \left(\sum_{i=1}^{k} \beta_{ki} n_i - b_k\right). \quad (10)$$

The partial derivatives of Eq. (10) for every species are set to zero to obtain the extremum point.

$$\Delta G_{i,f}^\theta + RT \ln\frac{P}{P^\theta} + RT \ln\frac{n_i}{\sum n_i} + \sum_{l=0}^{L} \lambda_k \beta_{ki} = 0. \quad (11)$$

Equation (11) is a system of equations containing $n + l$ unknown variables, for which the amount of species n_i (i = 1, 2, ..., n) and Lagrange multipliers λ_k (k = 1, 2, …, l) can be obtained.

The Aspen Plus V12 software was applied to calculate the equilibrium yield of catalytic pyrolysis. The IDEAL property method (Ideal gas and Raoult's Law) was used in this simulation because the process involves conventional low-pressure species.

3 Results and discussion

3.1 Thermodynamic analysis of reaction pathways

Based on the acid-catalyzed carbonium mechanism and previously mentioned hydrocarbon cracking pathway (Section 2.1), possible reaction pathways for $C_{5–8}$ *n*/*iso*/cyclo-paraffins in naphtha were proposed (Table S1). The detailed thermodynamic data for different reaction pathways were calculated based on Eqs. (5)–(8).

3.1.1 Reaction pathway of $C_{5–8}$ *n*-paraffins

Figures 1(a) and 1(b) depict the relationship of log K with reaction temperature for the removal of light olefins (ethylene, propylene, butene) and light paraffins (methane, ethane, propane, and butane) from $C_{5–8}$ *n*-paraffins by

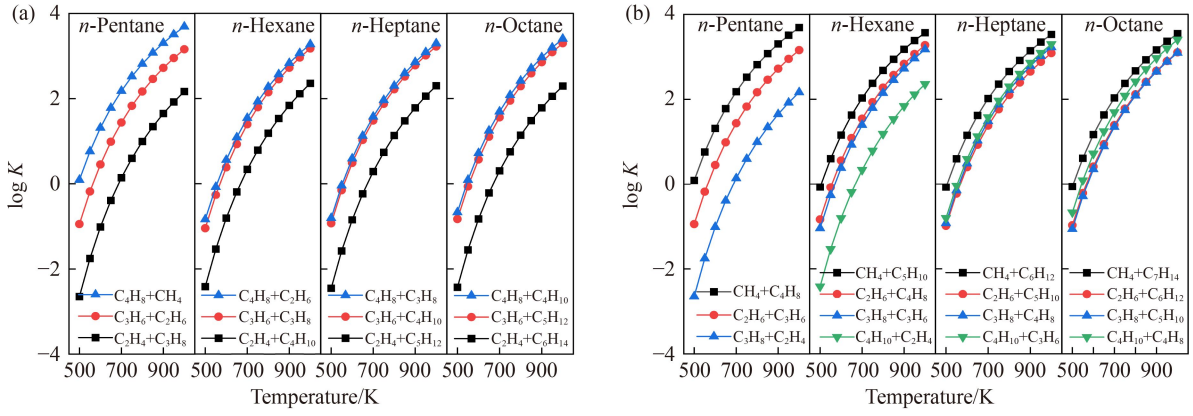

Fig. 1 Equilibrium constants for the protolytic cracking pathway of $C_{5–8}$ *n*-paraffins to form (a) light olefins and (b) light paraffins.

protolytic cracking pathway. The equilibrium constant for the cracking pathway of *n*-paraffins increases with increasing reaction temperature, owing to the endothermic nature of these reactions. The endothermic heat of protolytic cracking is approximately 60–100 kJ·mol^{-1}. For the cracking pathway, long-chain *n*-paraffins are more easily form light olefins by comparing the equilibrium constants of C_{5-8} *n*-paraffins to form the same olefins. For example, the equilibrium constants for protolytic cracking of *n*-pentane to form ethylene at 900 K is 44.68, while the *n*-octane is 60.62. Moreover, butene exhibits the highest equilibrium constant of formation, followed by propylene, and ethylene, indicating that butene is more easily formed than propylene and ethylene in the cracking pathway of *n*-paraffins.

The equilibrium constants of protolytic cracking pathway of C_{5-8} *n*-paraffins is less than one at 550 K, implying that the low conversion for the protolytic cracking pathway of *n*-paraffins at low temperatures. High temperature can promote the protolytic cracking pathway of C_{5-8} alkanes, but the formation of light olefins is accompanied by the formation of light paraffins. A comparison of the equilibrium constants for the cracking of C_{5-8} *n*-paraffins to form light paraffins (Fig. 1(b)), reveals that methane is easily formed during the cracking of C_{5-8} *n*-paraffins because the equilibrium constants for the cracking of the same reactants to methane are higher than those to other light paraffins (ethane, propane, and butane). Momayez et al. [42] also got similar results, where methane had the highest yield, followed by ethane, and propane in succession in their naphtha catalytic cracking experiments. Therefore, the formation of methane and other olefins molecular is more likely to occur for the protolytic cracking pathway of C_{5-8} *n*-paraffins.

Figure 2(a) presents the equilibrium constants for C_{5-8} *n*-paraffins undergoing C–H bond cleavage at different reaction temperatures. The endothermic heat of the dehydrogenation cracking pathway is approximately 130 kJ·mol^{-1}. The equilibrium constants for dehydrogenation cracking reactions of C_{5-8} *n*-paraffins are also similar, and the equilibrium constant is much lower than one at reaction temperatures is lower than 950 K. This indicates that the dehydrogenation cracking pathway of *n*-paraffins is extremely thermodynamically unfavorable. However, the dehydrogenation cracking step of *n*-paraffin does not produce light paraffin by-products, it is an ideal pathway for the catalytic pyrolysis of *n*-paraffins to form light olefins.

In addition to the protolytic cracking pathways of *n*-paraffins, the hydride transfer cracking pathway of C_{5-8} *n*-paraffins can also yield light paraffins. Figure 2(b) depicts the dependency of log *K* on the reaction temperature for hydride transfer cracking pathways of C_{5-8} *n*-paraffins. The equilibrium constants of hydride transfer between C_{5-8} *n*-paraffins and ethylene are relatively similar: they decrease with increasing temperature because all such reactions are exothermic reactions (the reaction enthalpy is about –13 kJ·mol^{-1}). The hydride transfer between C_{5-8} *n*-paraffins and propylene are all slightly endothermic reactions (the reaction enthalpy is about 0–2 kJ·mol^{-1}), and the equilibrium constants are all less than the equilibrium constants of C_{5-8} *n*-paraffins and ethylene within the calculated reaction temperature range. This indicates that the hydride transfer between C_{5-8} *n*-paraffins and propylene is more difficult than that between C_{5-8} *n*-paraffins and ethylene from the perspective of thermodynamics.

For the protolytic cracking pathways of *n*-paraffins, their equilibrium constants are higher than those of the dehydrogenation cracking pathway and the hydride transfer cracking pathway. Thus, the protolytic cracking pathway of *n*-paraffins is thermodynamically favorable.

3.1.2 Reaction pathway of C_{5-8} *iso*-paraffin

Figure 3 depicts the plot of log *K* against reaction temperatures for the C–C bond cleavage in C_{5-8} *iso*-paraffins. Similar to the protolytic cracking pathway of *n*-paraffins, long-chain olefins are more likely to form in the protolytic cracking pathway of *iso*-paraffins, and the

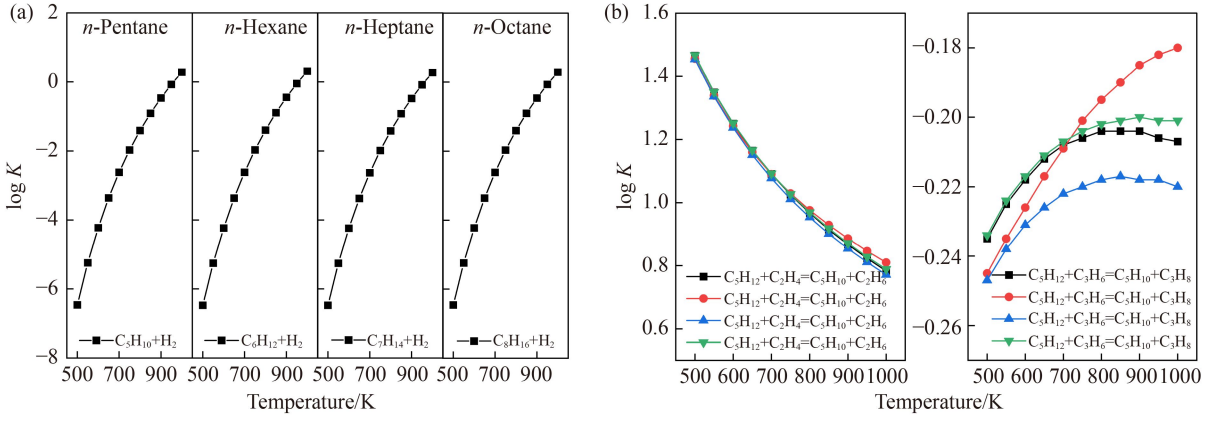

Fig. 2 Equilibrium constants for (a) dehydrogenation and (b) hydride transfer cracking pathways of C_{5-8} *n*-paraffins.

equilibrium constant decreases in the order of removal of methane, ethane, propane, and butane. The endothermic heat for protolytic cracking of *iso*-paraffin to form light paraffins is smaller than that of *n*-paraffins. For example, the endothermic heat for protolytic cracking of *n*-pentane to form methane at 900 K is 66.69 kJ·mol^{-1}, while the endothermic heat of *iso*-pentane is 56.95 kJ·mol^{-1}. On the other hand, the equilibrium constants demonstrate the opposite. For instance, the equilibrium constant of protolytic cracking of *iso*-pentane to form methane at 900 K is around 1.45 times greater than the equilibrium constant for the cracking of *n*-pentane to form methane. Moreover, the equilibrium constant for the formation of the same light olefins or light paraffins gradually increases as the chain length increases, indicating that long-chain *iso*-paraffins are more prone to protolytic cracking pathways.

The log *K* for the dehydrogenation cracking pathways of C_{5-8} *iso*-paraffins are illustrated in Fig. 4(a). The dehydrogenation cracking of *iso*-paraffins is strongly endothermic, and the reaction enthalpy is approximately 120 kJ·mol^{-1}. Consistent with the dehydrogenation cracking pathways of *n*-paraffins, the dehydrogenation cracking pathways of *iso*-paraffins are also thermodynamically unfavorable.

Figure 4(b) depicts the graph of log *K* versus reaction temperatures for hydride transfer cracking pathways of ethylene and propylene with C_{5-8} *iso*-paraffins. The equilibrium constant for the hydride transfer cracking pathway of *iso*-paraffins decreases with increasing reaction temperature because the hydride transfer of C_{5-8} *iso*-paraffins with ethylene and propylene is exothermic. The equilibrium constants for these reactions are also much larger than those for the dehydrogenation reactions. In comparison with the protolytic cracking pathway of *iso*-paraffins, the hydride transfer pathway dominates at low temperatures, while the cracking pathway dominates at high temperatures (> 600 K). Moreover, the equilibrium constants for hydride transfer between C_{5-8} *iso*-paraffins and ethylene are higher than those for propylene, indicating that the hydride transfer between ethylene and *iso*-paraffins is more thermodynamically favorable.

Among the protolytic, dehydrogenation, and hydride transfer cracking pathways of C_{5-8} *n*/*iso*-paraffins, the protolytic and hydride transfer cracking pathways yield

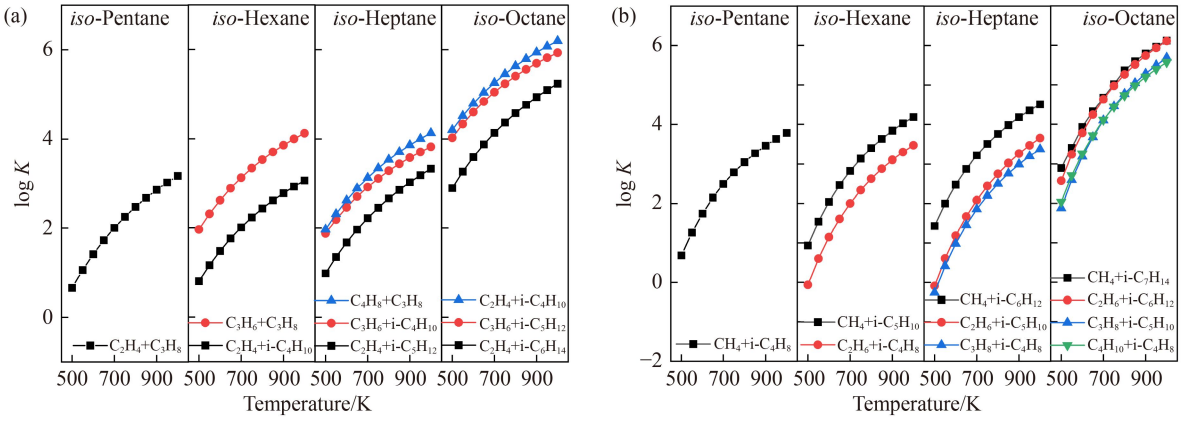

Fig. 3 Equilibrium constants for the protolytic cracking pathway of C_{5-8} *iso*-paraffins to form (a) light olefins and (b) light paraffins.

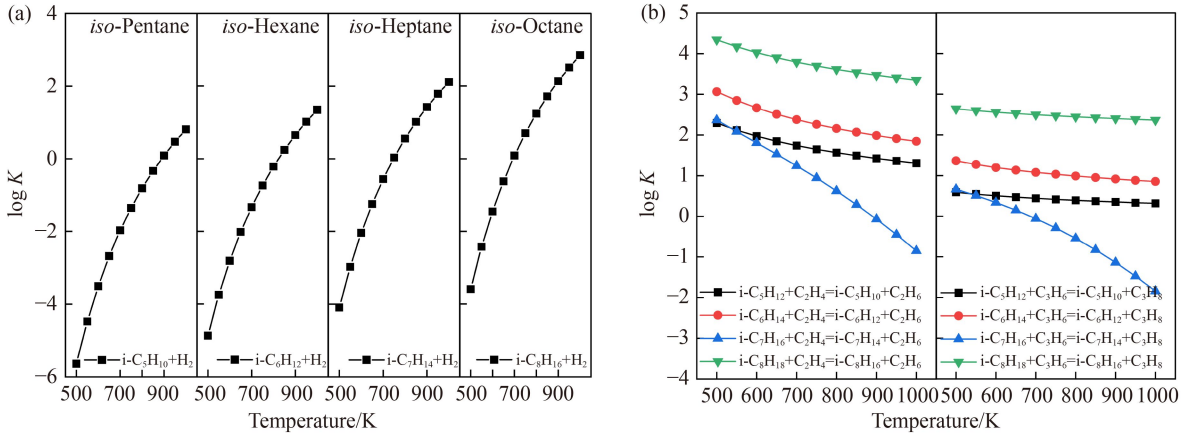

Fig. 4 Equilibrium constants for (a) dehydrogenation and (b) hydride transfer cracking pathways of C_{5-8} *iso*-paraffins.

light paraffins, resulting in a lower selectivity for light olefins. While the dehydrogenation cracking pathways generate hydrogen without other light paraffins. Unfortunately, the protolytic and hydride transfer cracking pathways of *n*/*iso*-paraffins are more thermodynamically favorable over HZSM-5 zeolites. Thus, a conversion of the protolytic and hydride transfer cracking pathways to dehydrogenation cracking pathways would result in the formation of larger amounts of light olefins, which are thus useful as a direction for future catalyst improvements, facilitating superior reaction pathways to enhance light olefins.

3.1.3 Reaction pathway of C_{5-8} cyclo-paraffins

The protolytic cracking of cyclo-paraffins results in the formation of two molecular olefins. Figure 5(a) illustrates the dependency of log *K* on the reaction temperature for the protolytic cracking pathway of C_{5-8} cyclo-paraffins. High carbon number cyclo-paraffins are more prone to protolytic cracking, and the equilibrium constants for the formation of two olefins with similar carbon numbers are higher. Moreover, the protolytic cracking pathway of cyclo-paraffin requires a higher reaction heat than *n*/*iso*-paraffin, approximately 130–180 kJ·mol^{-1}.

Dehydrogenation of cyclo-paraffins results in the formation of cyclo-olefins, which reduces the selectivity toward light olefins compared with the protolytic cracking pathway of cyclo-paraffins. Moreover, cyclo-olefins are precursors for the formation of aromatics, thus the dehydrogenation cracking pathways of cyclo-paraffins could result in the formation of aromatics. The endothermic heat of the dehydrogenation cracking pathway is similar to the dehydrogenation cracking pathways of C_{5-8} *n*/*iso*-paraffins, at approximately 120 kJ·mol^{-1}. Figure 5(b) depicts the log *K* for the dehydrogenation cracking of C_{5-8} cyclo-paraffins. The dehydrogenation cracking pathways of C_{5-8} cyclo-paraffins have a similar equilibrium constant over the calculated temperature range, and it is lower than those for the protolytic cracking pathway; hence, the dehydrogenation cracking pathway of cyclo-paraffins is less thermodynamically favorable.

Hydrogen transfer cracking pathways of ethylene and propylene with C_{5-8} cyclo-paraffins not only do not form light olefins, but also consume light olefin molecules. Figure 5(c) illustrates the dependency of log *K* on the reaction temperature for hydrogen transfer cracking pathways of ethylene and propylene with C_{5-8} cyclo-paraffins. The equilibrium constants for the hydrogen transfer cracking pathways of cyclo-paraffins are larger than those for the protolytic and dehydrogenation

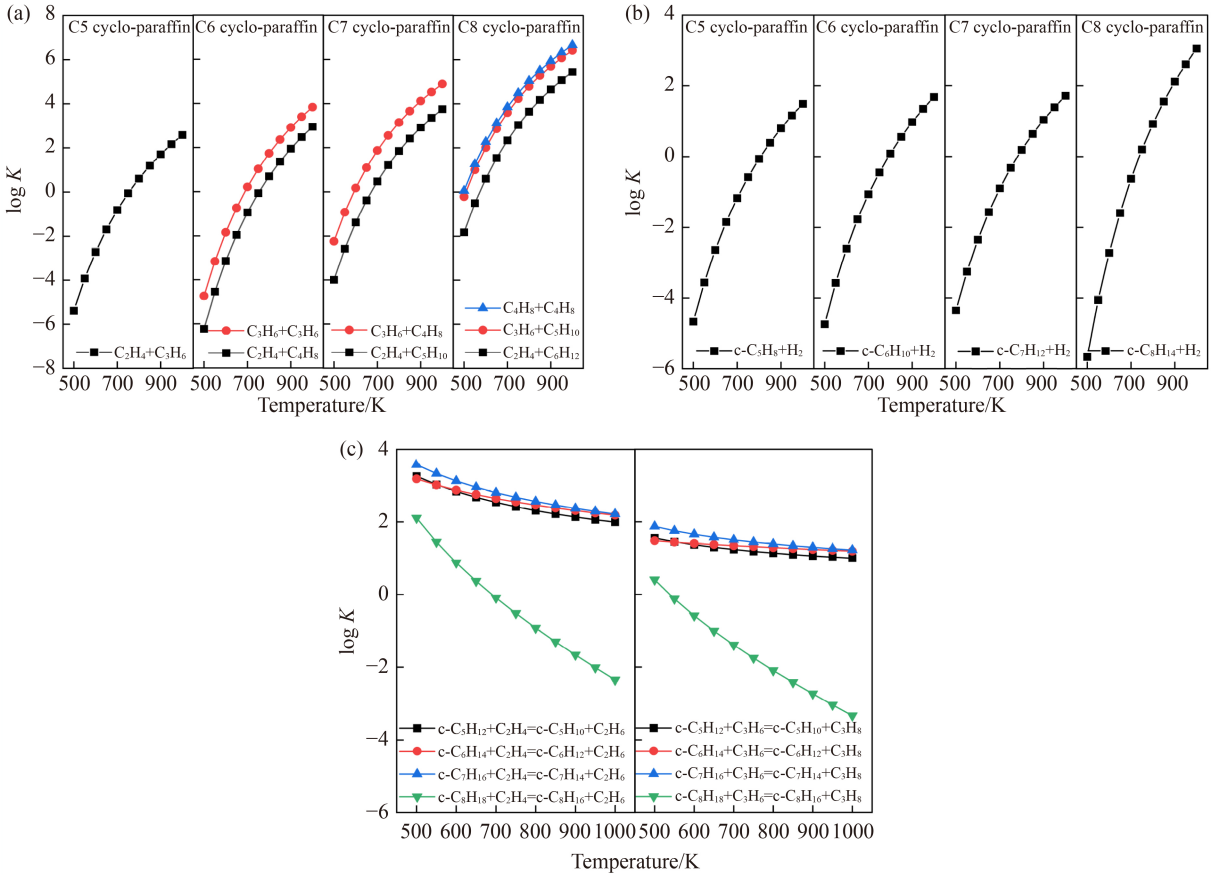

Fig. 5 Equilibrium constants for (a) protolytic, (b) dehydrogenation and (c) hydrogen transfer cracking pathways of C_{5-8} cyclo-paraffins.

cracking pathways at low temperature (< 800 K), which indicates that hydrogen transfer cracking pathways are more thermodynamically favorable for cyclo-paraffins (< 800 K). However, hydrogen transfer cracking pathways of ethylene and propylene with C_{5-8} cyclo-paraffins results in the formation of cyclo-olefins and light paraffins, which greatly reduces the selectivity of light olefins. Therefore, it is necessary to promote the protolytic cracking pathways of cyclo-paraffins, a conversion of the dehydrogenation and hydrogen transfer cracking pathways to protolytic cracking pathways would result in the formation of larger amounts of light olefins.

Based on the discussions above, the cracking pathways of *n*/*iso*-paraffins follow the same thermodynamic principle, whereas those of cyclo-paraffins are different. The protolytic cracking pathways of *n*/*iso*-paraffins on solid acid catalysts are the most thermodynamically favorable, followed by the hydride transfer and dehydrogenation cracking pathways. The hydrogen transfer cracking pathways of cyclo-paraffins on solid acid catalysts is most favorable thermodynamically as the temperature is less than 800 K, and the protolytic and dehydrogenation cracking pathways of cyclo-paraffins on solid acid catalysts are more difficult. However, the dehydrogenation cracking pathways of *n*/*iso*-paraffins and protolytic cracking pathways of cyclo-paraffins increase the selectivity for light olefins because no other by-products are produced. Therefore, it is important to develop catalysts that promote the dehydrogenation cracking pathways of *n*/*iso*-paraffins and the protolytic cracking pathways of cyclo-paraffins.

3.2 Thermodynamic analysis of equilibrium distributions

To clarify the reactivity and the effect of the coexistence of other hydrocarbons, the effects of thermodynamic factors on the equilibrium yields of C_{5-8} *n*/cyclo-paraffins systems were investigated in this section.

3.2.1 Equilibrium yield of C_{5-8} *n*-paraffin systems

The effect of reaction temperature on the equilibrium distribution of the catalytic pyrolysis of C_{5-8} *n*-paraffins is depicted in Fig. 6. The equilibrium yield increases with an increase in the carbon number due to their ability to remove more light hydrocarbons by scissions of chemical bonds. However, the equilibrium yield of pyrolysis products demonstrates a similar trend for *n*-paraffins with different carbon numbers. This indicates that the thermodynamic equilibrium rule of pyrolysis products is similar for different systems of C_{5-8} *n*-paraffins. The cracking and hydrogen transfer pathways of *n*-paraffins lead to high equilibrium yields of light paraffins,

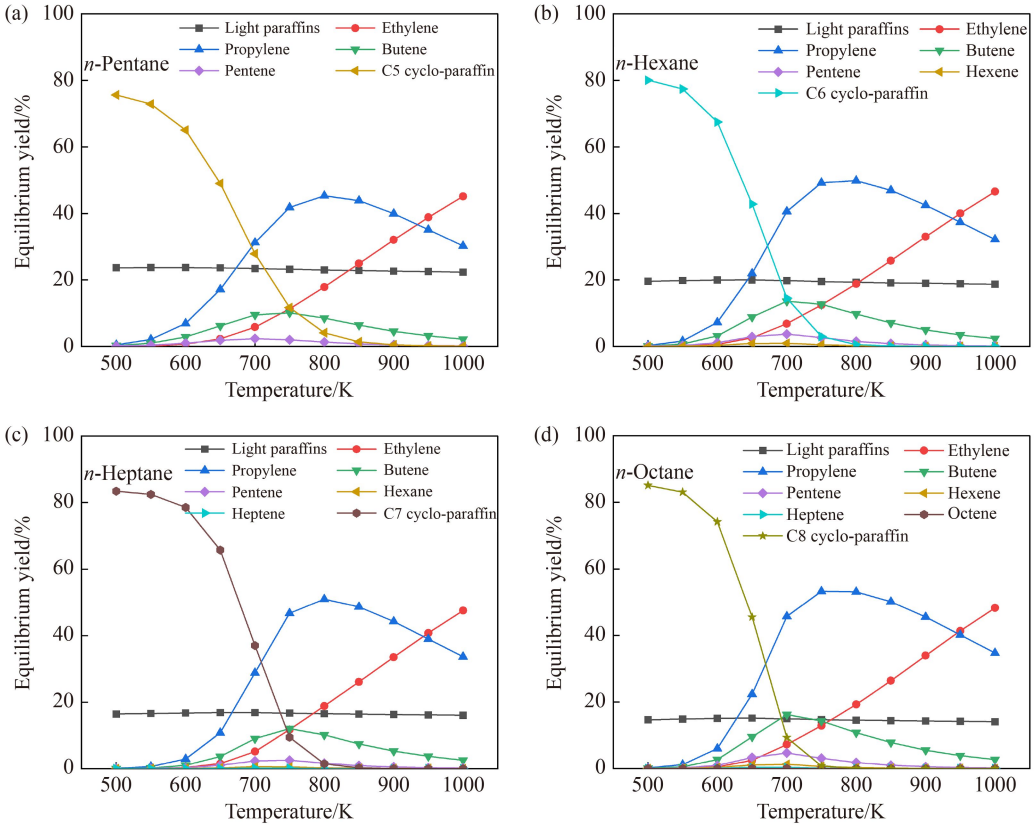

Fig. 6 Effects of temperature on thermodynamic equilibrium yield for (a) *n*-pentane, (b) *n*-hexane, (c) *n*-heptane and (d) *n*-octane at 0.1 MPa.

approximately 20 wt %. The ethylene equilibrium yield notably increases from ~0.02% at 500 K to 45.12% at 1000 K. C_{3-8} olefins demonstrate a maximum yield within the temperature range of 600 K–800 K, which is consistent with their role as an intermediate fraction in the reaction at high temperatures. The temperature corresponding to the maximum equilibrium yield of C_{3-8} olefins decreases with increasing carbon number.

Figure 7 indicates the preferential generation of C_{5+} olefins up to approximately 550 K, while ethylene and propylene become the dominant species at higher temperatures. The equilibrium yield of high-carbon-number olefins gradually decreases and approaches zero at reaction temperatures above 850 K. It can be deduced that olefins with high carbon numbers can be almost completely converted when the system attains thermodynamic equilibrium at a temperature above 850 K because the cracking reaction predominates at such a high temperature. This behavior stems from the trends followed by the Gibbs energy of formation. Lehmann et al. [33] studied the effects of temperature on Gibbs energies of formation of light olefins. It was found that C_{5+} olefins exhibit higher thermodynamic stability (smaller values of Gibbs energies of formation) compared with that exhibited by ethylene and propylene at lower temperatures, this relation is reversed at higher temperatures, which was consistent with the calculated results in the present work.

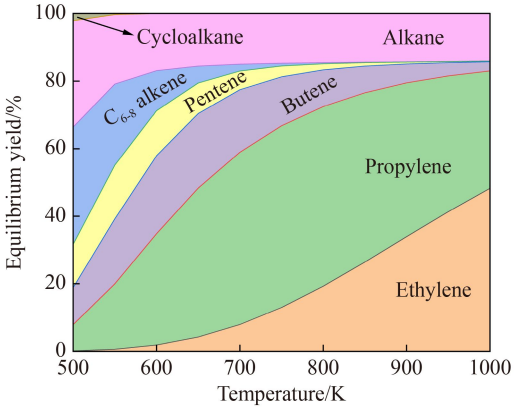

Fig. 7 Equilibrated olefin groups of C_{2-8} olefin systems at 0.1 MPa.

According to LeChatelier's principle, high pressure favors the formation of liquid products, and low pressure favors the formation of gaseous products [43]. Figure 8 illustrates the effects of the total hydrocarbon pressure on the equilibrium yields for the catalytic pyrolysis of C_{5-8} *n*-paraffins. The equilibrium yields of the pyrolysis products are similar for C_{5-8} *n*-paraffin systems. With an increasing total hydrocarbon pressure, the equilibrium yield of ethylene decreases while that of propylene reaches a maximum within the total hydrocarbon pressure

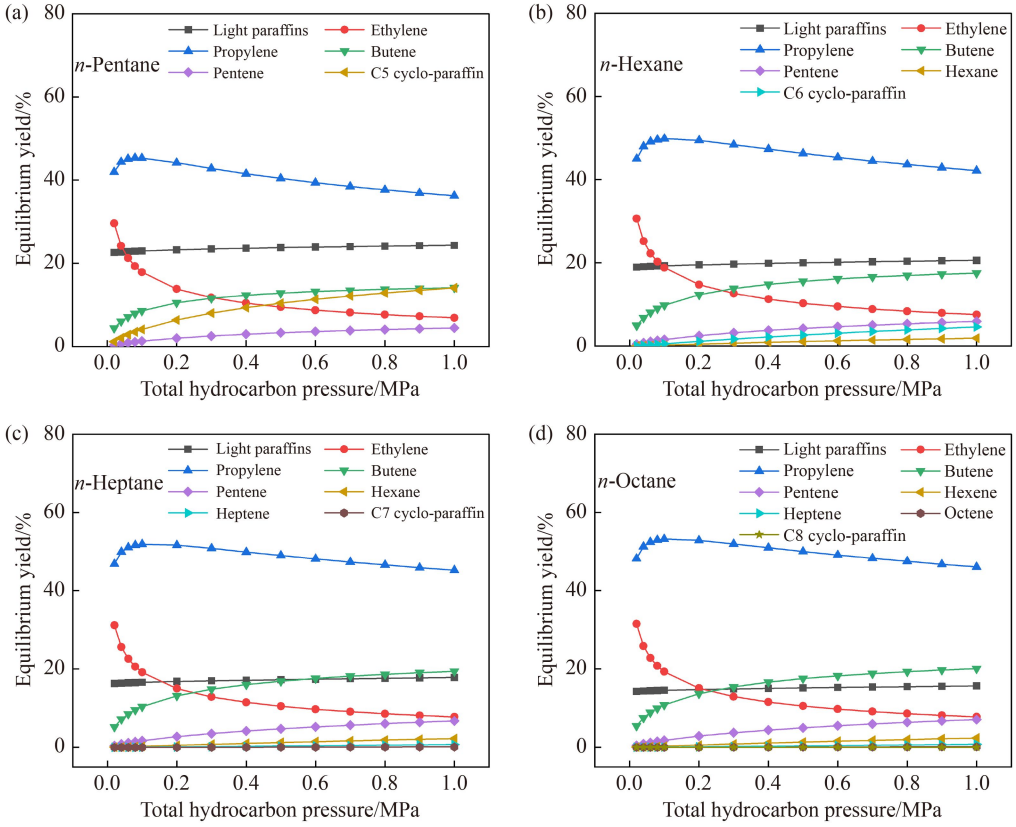

Fig. 8 Effects of total hydrocarbon pressure on thermodynamic equilibrium yield for (a) *n*-pentane, (b) *n*-hexane, (c) *n*-heptane, and (d) *n*-octane at 800 K.

at 0.1 MPa, increasing the equilibrium yield of C_{4+} pyrolysis products. Thus, cracking reactions are limited to a certain extent under high-pressure conditions. A total hydrocarbon pressure below 0.2 MPa is appropriate for improving the equilibrium yields of ethylene and propylene. For C_{5-8} *n*-paraffin systems, the equilibrium yields of ethylene and propylene from high-carbon-number *n*-paraffins are higher than those from low-carbon-number *n*-paraffins under the same total hydrocarbon pressure.

Based on the results obtained from thermodynamic calculations, a relatively high reaction temperature and low total hydrocarbon pressure are recommended to increase the equilibrium yield of light olefins. At high reaction temperatures and low total hydrocarbon pressures, high-carbon-number hydrocarbons have higher Gibbs free energies than the Gibbs free energies of low-carbon-number hydrocarbons, facilitating the occurrence of cracking reactions.

3.2.2 Equilibrium yield of C_{5-8} *n*-paraffin and cyclo-paraffin mixture systems

C_{5-8} *n*-paraffins and cyclo-paraffins mixtures were employed to explore the effects of the cyclo-paraffin content on equilibrium yields, as illustrated in Fig. 9. The products vary greatly after introducing the cyclo-paraffin into *n*-paraffin, an essential reason is that the cyclo-olefins could exhibit higher thermodynamic stability compared to light olefins. The introduction of cyclo-alkanes promotes the formation of the corresponding cyclo-olefins, this behavior stems from the hydrogen transfer cracking pathway of cyclo-paraffins. On the other hand, the introduction of cyclo-paraffin suppresses the formation of light olefins. In addition, the yield of light olefins for the mixture of high-carbon-number *n*-paraffins and cyclo-paraffins is higher than that for the mixture of low-carbon-number *n*-paraffins and cyclo-paraffins, and the difference in the yields of light olefins decreases with an increase in the carbon number.

The protolytic cracking pathways of cyclo-paraffins significantly enhance the yields of light olefins, because, stoichiometrically, cyclo-paraffins decompose into two olefins. To determine the corresponding limiting values of pyrolysis products considering the protolytic cracking pathway of cyclo-paraffin for paraffin and cyclo-paraffin system. *n*-Hexane and cyclohexane mixtures (50%:50%) were used to explore the effects of reaction temperature and total hydrocarbon pressure on the pyrolysis of *n*-paraffin and cyclo-paraffin mixtures because the content is similar for *n*-paraffins and cyclo-paraffins in naphtha, approximately 30%. Figures 10(a) and 10(b) display the joint effect of the reaction temperature and total hydrocarbon pressure on the equilibrium yields of ethylene and propylene for the catalytic pyrolysis of a mixture of C_6 *n*-paraffin and cyclo-paraffin. The effects

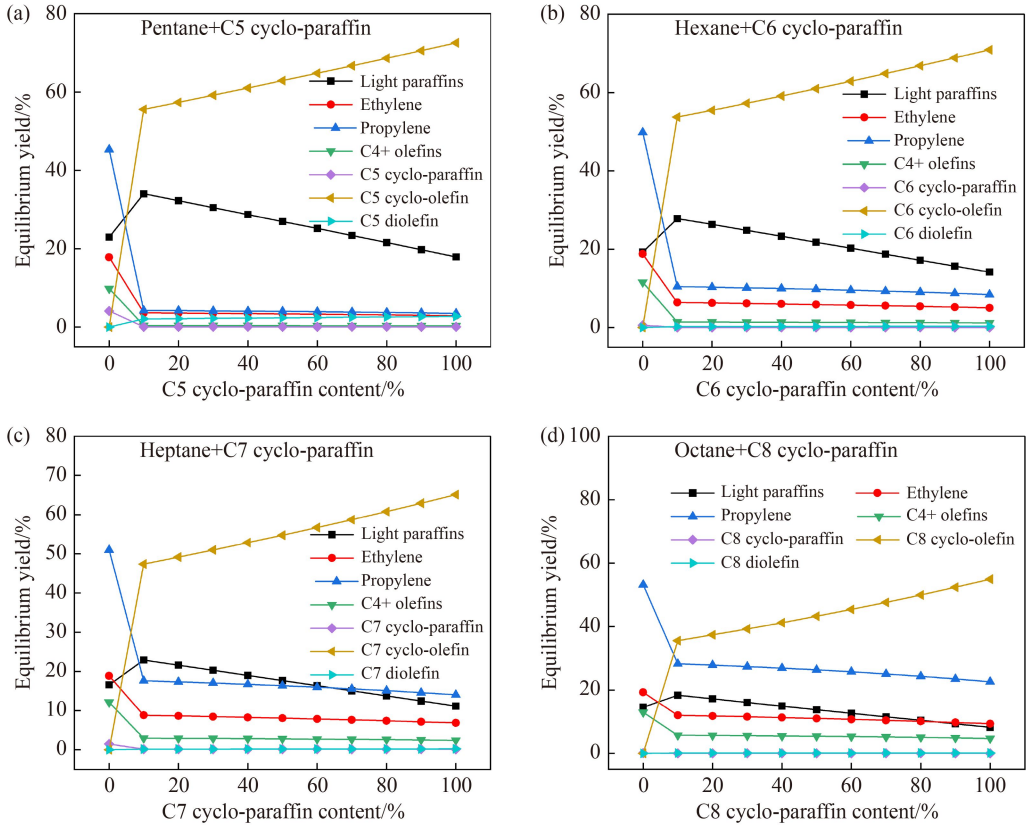

Fig. 9 Effect of cyclo-paraffin content on pyrolysis product of (a) *n*-pentane, (b) *n*-hexane, (c) *n*-heptane, and (d) *n*-octane.

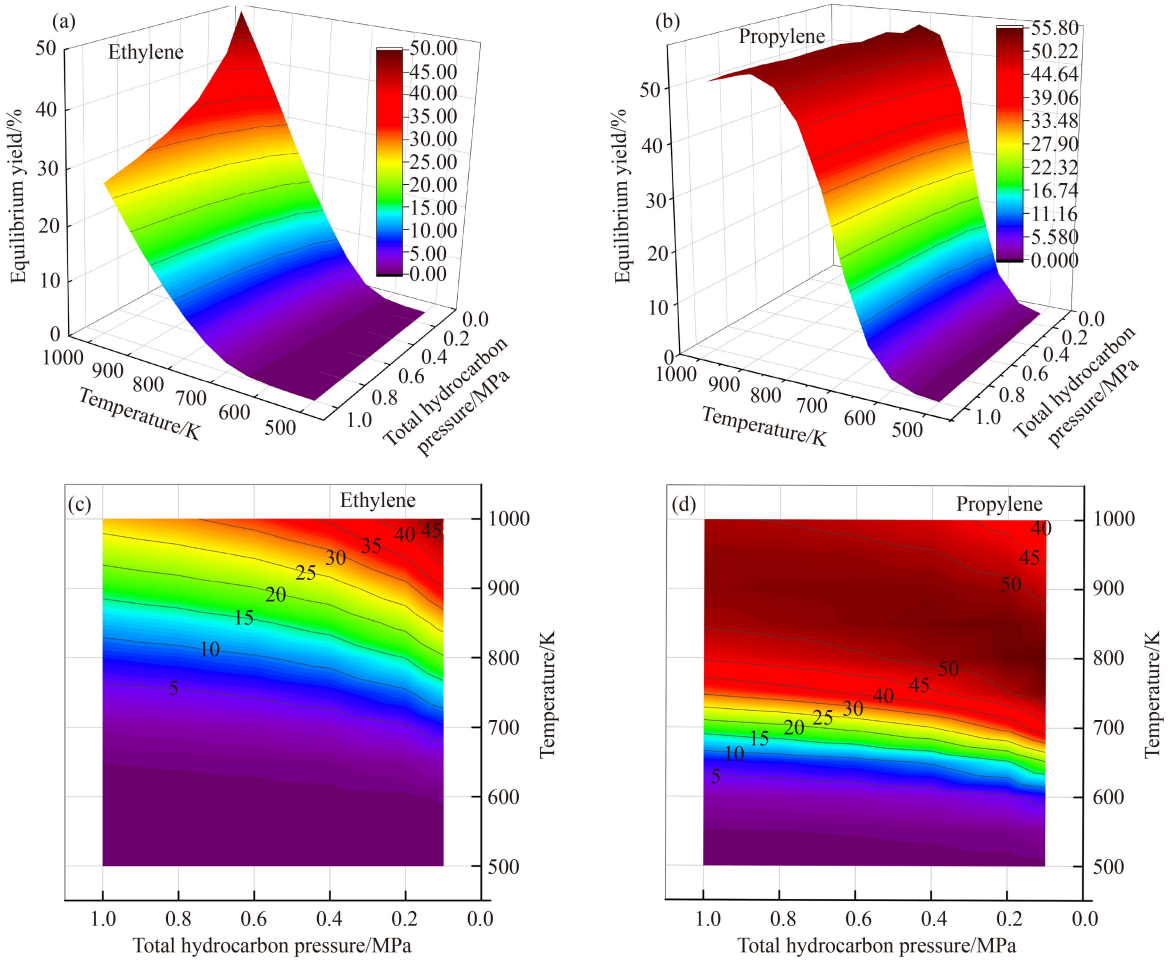

Fig. 10 The joint effect of temperature and pressure on the equilibrium yields of (a) ethylene and (b) propylene as well as contour maps of (c) ethylene and (d) propylene.

of temperature and total hydrocarbon pressure on the product distribution for the cracking of the *n*-paraffin and cyclo-paraffin mixtures are similar to those in single *n*-paraffins. The maximum ethylene and propylene yields are 49.90% and 55.77% at total hydrocarbon pressure of 0.1 MPa. Optimal reaction temperatures were found at 1000 K (ethylene) and 800 K (propylene), respectively.

To guide the selection of operation parameters for catalytic pyrolysis of *n*-paraffins and cyclo-paraffins mixtures, the operating maps (Figs. 10(c) and 10(d)) of ethylene and propylene for the reaction temperature and total hydrocarbon pressure were constructed and analyzed. Contour maps were plotted using the equilibrium yields of ethylene and propylene. As can be inferred, the temperature is the most important factor affecting product distribution. High temperatures and low pressures favor the formation of ethylene, and moderate temperatures and low pressures favor the formation of propylene. To achieve ethylene yields above 20%, temperatures above 800 K are required. At the same time, an optimum propylene yield (approximately 50%) can be observed at 750–900 K.

4 Conclusions

In this work, C_{5-8} *n*/*iso*/cyclo-paraffins, the primary species of naphtha, were selected to investigate the thermodynamic properties of reaction pathways occurring over solid acid catalysts, including protolytic, dehydrogenation, and hydride/hydrogen transfer cracking pathways. Based on the analysis, it can be concluded that *n*/*iso*-paraffins are ideal feedstocks for the catalytic cracking of naphtha to produce light olefins, whereas cyclo-paraffins are non-ideal feedstocks. It is necessary to develop catalysts that promote the dehydrogenation cracking pathways of *n*/*iso*-paraffins and protolytic cracking pathways of cyclo-paraffins to enhance the yield of light olefins. However, the protolytic cracking pathways of *n*/*iso*-alkanes and the hydrogen transfer cracking pathways of cyclo-alkanes are unavoidable. Therefore, there are two issues worth considering: (1) the comprehensive utilization of light paraffin by-products; (2) the content of cyclo-paraffins in pyrolysis feedstocks. The effects of thermodynamic factors on the thermodynamic equilibrium yield demonstrated similar

trends for C_{5-8} *n*-paraffin and cyclo-paraffin systems, and the increase of chain length could promote the equilibrium yield of pyrolysis products. The optimum reaction conditions that maximize the yields of light olefins are reaction temperatures between 750 and 900 K and total hydrocarbon pressure is 0.1 MPa.

Acknowledgements The authors acknowledge the support from the National Natural Science Foundation of China (Grant No. 22021004) and the National Key Research and Development Program of China (Grant No. 2020YFA0210900)

Electronic Supplementary Material Supplementary material is available in the online version of this article at https://dx.doi.org/10.1007/s11705-022-2207-6 and is accessible for authorized users.

Nomenclature

$\Delta_f H_m^\theta$	Standard molar formation enthalpy, kJ
T	Reaction temperature, K
$C_{p,m}$	Molar heat capacity at constant pressure, $J \cdot mol^{-1} \cdot K^{-1}$
$\Delta_f S_m^\theta$	Standard molar formation entropy, $J \cdot K^{-1}$
$C_{p,m,i}$	Contribution value of each group to the $C_{p,m}$
N_i	The number of groups
$\Delta_r H_m^\theta$	Standard molar reaction enthalpy, kJ
$\Delta_r S_m^\theta$	Standard molar reaction entropy, $J \cdot K^{-1}$
$\Delta_r G_m^\theta$	Standard molar reaction Gibbs free energy, kJ
K^θ	Standard equilibrium constant
R	Molar gas constant, $J \cdot mol^{-1} \cdot K^{-1}$
G_t	Total Gibbs free energy of mixed system, kJ
n_i	Numbers of moles of species *i*
μ_i	Chemical potential of species *i*
λ_k	Lagrange multiplier of the *k*th element
β_{ki}	Number of atoms of the *k*th element in a mole of the *i*th species
b_k	Total moles of the *k*th element, mol
$\Delta G_{i,f}^\theta$	Standard mole generation Gibbs free energy of species *i*, $kJ \cdot mol^{-1}$
P	Total hydrocarbon pressure, MPa
P^θ	Standard pressure, MPa

References

1. Kubo K, Takahashi T, Iida H, Namba S, Igarashi A. Reactivities of C_{6-8} hydrocarbons and effect of coexistence of another hydrocarbon in cracking on H-ZSM-5 catalyst at high temperatures. Applied Catalysis A: General, 2014, 482: 370–376
2. Wattanapaphawong P, Reubroycharoen P, Mimura N, Sato O, Yamaguchi A. Effect of carbon number on the production of propylene and ethylene by catalytic cracking of straight-chain paraffins over phosphorus-modified ZSM-5. Fuel Processing Technology, 2020, 202: 106367
3. Ren L, Wang B, Lu K, Peng R, Guan Y, Jiang J, Xu H, Wu P. Selective conversion of methanol to propylene over highly dealuminated mordenite: Al location and crystal morphology effects. Chinese Journal of Catalysis, 2021, 42(7): 1147–1159
4. Bai Y, Zhang G, Liu D, Zhang Y, Zhao L, Gao J, Xu C, Meng Q, Gao X. The advance in catalytic pyrolysis of naphtha technology using ZSM-5 as catalyst. Applied Catalysis A: General, 2021, 628: 118399
5. Chen F, Hao J, Yu Y, Cheng D, Zhan X. The influence of external acid strength of hierarchical ZSM-5 zeolites on *n*-heptane catalytic cracking. Microporous and Mesoporous Materials, 2022, 330: 111575
6. Chen X, Zhang X, Qin R, Shan S, Xia P, Li N, Pu J, Liu J, Liu Y, Yang C. Distribution of nitrogen and oxygen compounds in shale oil distillates and their catalytic cracking performance. Petroleum Science, 2020, 17: 1764–1778
7. Cheng Q, Shen B, Sun H, Zhao J, Liu J. Methanol promoted naphtha catalytic pyrolysis to light olefins on Zn-modified high-silicon HZSM-5 zeolite catalysts. RSC Advances, 2019, 9(36): 20818–20828
8. Ng S H, Heshka N E, Lay C, Little E, Zheng Y, Wei Q, Ding F. FCC coprocessing oil sands heavy gas oil and canola oil. 2. Gasoline hydrocarbon type analysis. Green Energy & Environment, 2018, 3(3): 286–301
9. Ng S H, Heshka N E, Zheng Y, Wei Q, Ding F. FCC coprocessing oil sands heavy gas oil and canola oil. 3. Some cracking characteristics. Green Energy & Environment, 2019, 4(1): 83–91
10. Ding J, Xue T, Wu H, He M. One-step post-synthesis treatment for preparing hydrothermally stable hierarchically porous ZSM-5. Chinese Journal of Catalysis, 2017, 38(1): 48–57
11. Pouria R, Vafi L, Karimzadeh R. Propane catalytic cracking on pretreated La-ZSM-5 zeolite during calcination for light olefins production. Journal of Rare Earths, 2017, 35(6): 542–550
12. Meng X, Xu C, Gao J, Li L. Studies on catalytic pyrolysis of heavy oils: reaction behaviors and mechanistic pathways. Applied Catalysis A: General, 2005, 294(2): 168–176
13. Whitmore F C. Mechanism of the polymerization of olefins by acid catalysts. Industrial & Engineering Chemistry, 1934, 26(1): 94–95
14. Hansford R C. A mechanism of catalytic cracking. Industrial & Engineering Chemistry, 1947, 39(7): 849–852
15. Fu Y, Ni Y, Cui W, Fang X, Chen Z, Liu Z, Zhu W, Liu Z. Insights into the size effect of $ZnCr_2O_4$ spinel oxide in composite catalysts for conversion of syngas to aromatics. Green Energy & Environment, 2021, in press
16. Li J, Li T, Ma H, Sun Q, Ying W, Fang D. Effect of nickel on phosphorus modified HZSM-5 in catalytic cracking of butene and pentene. Fuel Processing Technology, 2017, 159: 31–37
17. Lin L F, Zhao S F, Zhang D W, Fan H, Liu Y M, He M Y. Acid strength controlled reaction pathways for the catalytic cracking of 1-pentene to propene over ZSM-5. ACS Catalysis, 2015, 5(7): 4048–4059
18. Caeiro G, Carvalho R H, Wang X, Lemos M A N D A, Lemos F, Guisnet M, Ribeiro F R. Activation of C_2–C_4 paraffins over acid and bifunctional zeolite catalysts. Journal of Molecular Catalysis A: Chemical, 2006, 255(1–2): 131–158

19. Lukyanov D B, Gnep N S, Guisnet M R. Kinetic modeling of propane aromatization reaction over HZSM-5 and GaHZSM-5. Industrial & Engineering Chemistry Research, 1995, 34(2): 516–523
20. Liu D, Cao L, Zhang G, Zhao L, Gao J, Xu C. Catalytic conversion of light paraffins to aromatics by metal-containing HZSM-5 zeolite catalysts—a review. Fuel Processing Technology, 2021, 216: 106770
21. Hou X, Qiu Y, Zhang X, Liu G. Analysis of reaction pathways for *n*-pentane cracking over zeolites to produce light olefins. Chemical Engineering Journal, 2017, 307: 372–381
22. Rahimi N, Karimzadeh R. Catalytic cracking of hydrocarbons over modified ZSM-5 zeolites to produce light olefins: a review. Applied Catalysis A: General, 2011, 398(1–2): 1–17
23. Nakasaka Y, Okamura T, Konno H, Tago T, Masuda T. Crystal size of MFI-type zeolites for catalytic cracking of *n*-hexane under reaction-control conditions. Microporous and Mesoporous Materials, 2013, 2182: 244–249
24. Wang R, Li Y, Jiang G, Zhang Y, Zhao Z, Xu C, Duan A, Wang Y. An efficient head-tail co-conversion process for high quality gasoline via rational catalytic cracking. Chemical Engineering Journal, 2020, 396: 125210
25. Wang Y, Jiang P, Zhu Y. A novel global reaction modeling approach considering the effects of pressure on pyrolysis of *n*-decane at supercritical pressures. Fuel, 2021, 287: 119416
26. Kubo K, Iida H, Namba S, Igarashi A. Selective formation of light olefin by *n*-heptane cracking over HZSM-5 at high temperatures. Microporous and Mesoporous Materials, 2012, 149(1): 126–133
27. Konno H, Okamura T, Kawahara T, Nakasaka Y, Tago T, Masuda T. Kinetics of *n*-hexane cracking over ZSM-5 zeolites—effect of crystal size on effectiveness factor and catalyst lifetime. Chemical Engineering Journal, 2012, 207–208: 490–496
28. Mochizuki H, Yokoi T, Imai H, Namba S, Kondo J N, Tatsumi T. Effect of desilication of H-ZSM-5 by alkali treatment on catalytic performance in hexane cracking. Applied Catalysis A: General, 2012, 449: 188–197
29. Hou X, Ni N, Wang Y, Zhu W, Qiu Y, Diao Z, Liu G, Zhang X. Roles of the free radical and carbenium ion mechanisms in pentane cracking to produce light olefins. Journal of Analytical and Applied Pyrolysis, 2019, 138: 270–280
30. Zhu T, Liang H, Zhang B, Tian Y, Liu G. Controllably tailoring external surface sites of nanosheet HZSM-5 for maximizing light olefins in catalytic cracking of *n*-decane. Chinese Journal of Chemical Engineering, 2021, 38: 276–285
31. Zhai P, Zheng J, Zhang J, Wang H, Qin Y, Liu H, Song L. Insight into reaction path and mechanism of catalytic cracking of *n*-hexane in HZSM-5 zeolites. Journal of Fuel Chemistry & Technology, 2021, 49(10): 1522–1530
32. Zhu X, Song Y, Li H, Liu S, Sun X, Xu L. Study on thermodynamics of butene catalytic cracking to propene and ethene. Chinese Journal of Catalysis, 2005, 26: 111–117 (in Chinese)
33. Lehmann T, Seidel-Morgenstern A. Thermodynamic appraisal of the gas phase conversion of ethylene or ethanol to propylene. Chemical Engineering Journal, 2014, 242: 422–432
34. Fu K, Chen M. Evaluation on migration of radioactive metal in irradiated graphite waste during an innovative thermal treatment based upon the Gibbs free energy minimization. Petroleum Science, 2022, 147: 10145–10161
35. Liu D, Zhang L, Zhang B, Bai Y, Zhao L, Gao J, Xu C, Liu H, Liu X. Analysis of thermodynamic equilibrium yield and process simulation for catalytic pyrolysis of light hydrocarbons based on one set of independent reactions. Chemical Engineering Science, 2022, 257: 117718
36. Dalmazzone D, Salmon A, Guella S. A second order group contribution method for the prediction of criticalntemperatures and enthalpies of vaporization of organic compounds. Fluid Phase Equilibria, 2006, 242(1): 29–42
37. Benson S W, Buss J H. Additivity rules for the estimation of molecular properties. thermodynamic properties. Journal of Chemical Physics, 1958, 29(3): 546–572
38. Sharma V, Agarwal V K. Equilibrium modeling and optimization for gasification of high-ash indian coals by the Gibbs free energy minimization method. Process Integration and Optimization for Sustainability, 2019, 3(4): 487–504
39. Huang H, Li Z, Ni W. The Gibbs reactor model and its realization on the computer. Power Engineering, 2004, 24: 902–907 (in Chinese)
40. Ghassemi H, Shahsavan-Markadeh R. Effects of various operational parameters on biomass gasification process; a modified equilibrium model. Energy Conversion and Management, 2014, 79: 18–24
41. Koukkari P, Pajarre R. Introducing mechanistic kinetics to the Lagrangian Gibbs energy calculation. Computers & Chemical Engineering, 2006, 30(6–7): 1189–1196
42. Momayez F, Darian J T, Sendesi S M T. Synthesis of zirconium and cerium over HZSM-5 catalysts for light olefins production from naphtha. Journal of Analytical and Applied Pyrolysis, 2015, 112: 135–140
43. Hansen R C. Thermodynamic changes, kinetics, equilibrium, and LeChatelier's principle. Journal of Chemical Education, 1984, 61(9): 804